
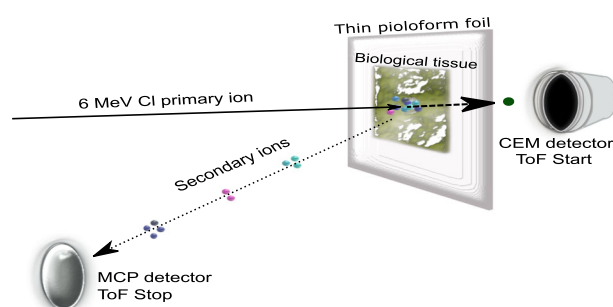


MeV-SIMS TOF Imaging of Organic Tissue with Continuous Primary Beam

Boštjan Jenčič,¹ Primož Vavpetič,¹ Mitja Kelemen,¹ Matjaž Vencelj,¹
Katarina Vogel-Mikuš,^{1,2} Anja Kavčič,² Primož Pelicon¹ 

¹Jožef Stefan Institute, Jamova 39, SI-1000, Ljubljana, Slovenia

²Biotechnical Faculty, Department of Biology, University of Ljubljana, Večna pot 11, SI-1000, Ljubljana, Slovenia



Abstract. MeV-SIMS is an emerging mass spectrometry imaging method, which utilizes fast, heavy ions to desorb secondary molecules. High yields and low fragmentation rates of large molecules, associated with the electronic sputtering process, make it particularly useful in biomedical research, where insight into distribution of organic molecules is needed. Since the implementation of MeV-SIMS into the micro-beam line at the tandem accelerator of Jožef Stefan Institute,

MeV-SIMS provided some valuable observations on the distribution of biomolecules in plant tissue, as discussed by Jenčič et al. (Nucl. Inst. Methods Phys. Res. B. **371**, 205–210, 2016; Nucl. Inst. Methods Phys. Res. B. **404**, 140–145, 2017). However, limited focusing ability of the chlorine ion beam only allowed imaging at the tissue level. In order to surpass shortcomings of the existing method, we introduced a new approach, where we employ a continuous, low-current primary beam. In this mode, we bombard thin samples with a steady chlorine ion flux of approx. 5000 ions/s. After desorbing molecules, chlorine ions penetrate through the thinly cut sample and trigger the time-of-flight “start” signal on a continuous electron multiplier detector, positioned behind the sample. Such bombardment is more effective than previously used pulsing-beam mode, which demanded several orders of magnitude higher primary ion beam currents. Sub-micrometer focusing of low-current primary ion beam allows imaging of biological tissue on a subcellular scale. Simultaneously, new time-of-flight acquisition approach also improves mass resolution by a factor of 5. Within the article, we compare the performance of both methods and demonstrate the application of continuous mode on biological tissue. We also describe the thin sample preparation protocol, necessary for measurements with low primary ion currents.

Keywords: MeV-SIMS, Time-of-flight, Electronic sputtering, Molecular imaging, Imaging mass spectrometry

Received: 19 March 2019/Revised: 23 May 2019/Accepted: 23 May 2019/Published Online: 27 June 2019

Introduction

The value of molecular imaging has increased significantly within the last decade. Numerous biomedical researches seek the identification and lateral distribution of molecules in living organisms [1–4]. Several cases of molecular imaging use can be seen in studies of drug metabolism in pharmaceutical research [5–8], as well as plant [9, 10], animal [11], and human physiology [12, 13].

Secondary ion mass spectrometry (SIMS) [14] is among the most widely employed mass spectroscopy imaging (MSI) techniques. It engages ions or ionic clusters with energies ranging between 0.5 and 30 keV to desorb particles from the investigated sample. Although praised for its excellence in lateral and mass resolution capabilities, compared to other MSI techniques such as DESI (desorption electrospray ionization) [15] and MALDI (matrix-assisted laser desorption ionization) [16–18], SIMS experiences difficulties in providing higher yields of heavier, non-fragmented, secondary ions. Difficulties in desorbing heavy secondary ions are partially solved by using large clustered primary ions, such as C_{60} [19] and Ar_n ($n = 60\text{--}30,000$) [20].

Correspondence to: Primož Pelicon; e-mail: primoz.pelicon@ijs.si

In order to overcome such problems in a different manner, another approach was taken by a novel SIMS method, using high-energy, heavy (swift) ions, MeV-SIMS [14, 21–23]. Although the basic principles of such analytical method are very similar to the original SIMS technique, the formation of secondary ions is caused by a different desorption process. While in the case of (keV) SIMS, secondary ions are desorbed through nuclear collisions (collision cascades); the desorption process with MeV-SIMS is governed by electron excitations, which results in higher yields and softer sputtering of heavier molecules, even compared to C_{60} keV primary ion clusters [24–27].

MeV-SIMS method has been implemented [28] using the high-energy focused beam from 2 MeV tandem accelerator [29] at the Jožef Stefan Institute (JSI) to complement extensive biomedical research based on elemental mapping with micro-PIXE [30–32]. Also, considering the available focusing power of standard Oxford Microbeams triplet lens, MeV-SIMS is generally executed by ^{35}Cl ions with charge states 5+, 6+, or 7+ and energies ranging between 5 MeV and 12 MeV. The energy and charge of the primary ion beam are customized by the needs of the research, with lower energy ions being more appropriate to the needs of better focusing characteristics, associated with higher lateral resolution, and higher energy ions being used, when we sought for higher yields of non-fragmented heavier molecular ions (i.e., $m/z > 2000$ Da). Due to the best compromise between available brightness, focusing ability, and associated stopping power, the most commonly used ions for the molecular imaging with MeV-SIMS at JSI are $^{35}\text{Cl}^{6+}$ with an energy of 5.8 MeV.

Originally, the method was conducted by pulsing the primary ion beam. Sample, residing in vacuum of about 5×10^{-7} m bar, was bombarded by short pulses of chlorine primary ions, generated by the parallel plate deflector. One of the plates was constantly biased at approx. 900 V, while the voltage on the other was switching from 0 to 900 V. The pulsing of the beam arose every 100 μs and the 900 V voltage effectively lasted from 20 to 100 ns, which was reflected in the duration of the primary ion pulse. Start of the voltage pulse at the deflector also served as a “start” signal to measure the time-of-flight of desorbed molecular ions. The energy of desorbed secondary ions was determined by the bias, applied to the sample holder, which amounts to most common values of +3 kV in positive and –5 kV in negative ion detection mode. The time elapsed between desorption of the molecule and detection of the same molecule by the microchannel plate (MCP) detector, positioned at the end of 1-m long drift space, depends on the mass and charge of the molecular ion.

The 3 MeV proton beam, used for extensive elemental tissue mapping with micro-PIXE at JSI, can be currently focused down to $0.6 \times 0.6 \mu\text{m}^2$ for high-current micro-PIXE elemental imaging due to high brightness of multicusp ion source [29]. Such a beam in combination with frozen hydrated tissue preparation technology [30, 32] enables quality elemental imaging with micro-PIXE at the subcellular level. In contrast to the proton beam, 5.8 MeV $^{35}\text{Cl}^{6+}$ beam could only be focused to approx. $15 \times 15 \mu\text{m}^2$,

as the limiting factor is the brightness of the sputtering source. Such lateral resolution enabled molecular imaging with MeV-SIMS at the tissue level only, discriminating distinctive tissue morphological structures. The time-of-flight (TOF) mass spectrometer can provide mass spectra of molecules with masses of up to 4000 μ , due to limited secondary ion acceleration voltage. Future application of higher voltages, both at the sample holder and higher post-acceleration voltage on the MCP detector, should greatly enhance the upper mass detection limit and shift the main limiting factor towards the physical process of electronic sputtering. The mass resolution of the pulsed MeV-SIMS mode was capped mainly by the length of the primary ion pulses shaped by the beam deflection device. Currently, the achievable mass resolution using such mode is estimated at the value of 350 for the m/z value of 300 μ .

Use of Continuous Primary Ion Beam

The existing setup of MeV-SIMS offers some advantages over other molecular imaging techniques such as conventional SIMS, but the limitations of mass and lateral resolution make it only partially applicable for uses in advanced biomedical investigations. The mass resolution of spectra is mainly influenced by the pulsing regime. The length of pulses has a lower limit at $dt = 20$ ns, which is equal to time-of-flight uncertainty of sputtered molecules. Since it takes approximately $t = 10 \mu\text{s}$ for most molecules to drift from the sample to the MCP detector, the time resolution cannot exceed the limit of $10 \mu\text{s} / 20 \text{ ns} = 500$ by much. We can therefore conclude that our current mass resolution, $m/dm = \frac{1}{2} t/dt$, is already at the higher limit and it cannot be improved significantly with the existing setup.

In order to overcome such restrictions, we introduced a new “start” signal. Instead of triggering the TOF measurement simultaneously with pulse of the primary ion beam, which only vaguely suggests the start of the desorption process, we decided to detect incoming ions directly. One can do that by detecting transmitted primary ions behind the sample, similar to the idea proposed by Siketić et al. [33]. By placing a continuous electron multiplier (CEM) behind the sample (Figure 1), the time uncertainty of start signal will become almost irrelevant if the samples are thin enough to allow the transmission of primary ions. The CEM will operate at bias of about 2400 V, which is enough to detect vast majority of incoming ions. Lower applied voltages on the CEM result in a position-dependent signal of primary ions.

The additional advantage of detecting the transmitted ions is the opportunity of utilizing lower primary ion currents. With the pulsed primary beam, ions were only bombarding the sample in approx. factor 10^{-4} of the total time of the measurement. Therefore, the absolute primary ion current had to be held high enough in order to maintain some reasonable count rate at the MCP detector. By operating with the continuous primary beam (also proposed in [23]), we may reduce the

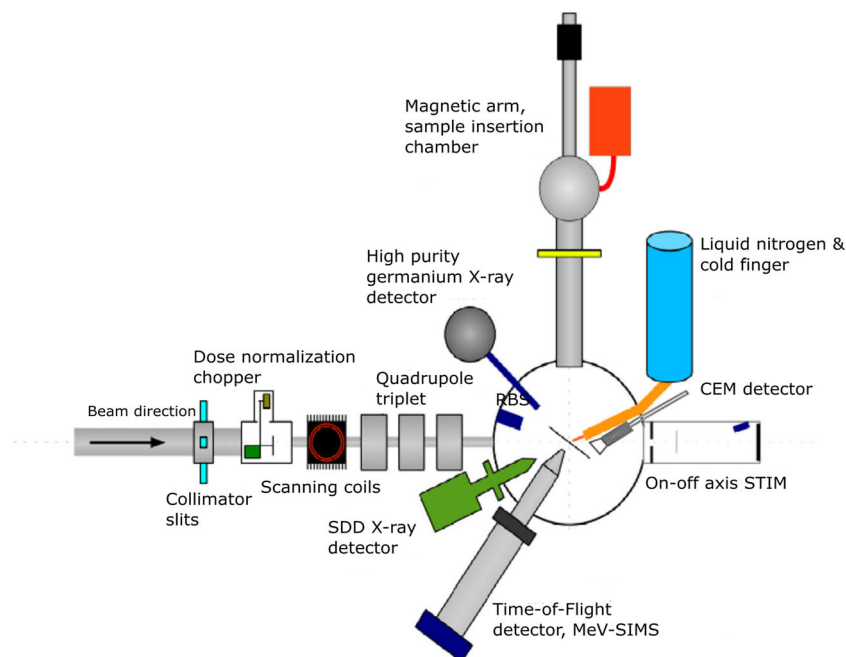


Figure 1. The scheme of experimental chamber at the JSI micro-beam line. CEM detector is positioned behind the sample holder on axis of primary ions

primary beam current to a value of approx. 5000 ions/s. To attain such low primary ion current, the object and collimator slits along the beamline, which dictate the size of the incoming ion beam, can be closed to a much smaller dimensions, allowing sub-micrometer lateral resolution.

The main challenge with this new approach is the sample preparation, so imaging with continuous beam is not applicable for any biological material of interest. Since 5 MeV ions can penetrate through only about 5 μm of organic tissue, samples should be prepared in a form of thin slice. However, most biological tissues can be prepared accordingly to the demands of the new continuous beam method. Thinly cut tissue samples are deposited on a thin pioloform material with thickness of approx. 100 nm. Pioloform is pre-coated on both sides by approx. 7 nm of carbon to become electrically conductive and allows for equipotential definition in the sample plane. Since carbon coating results in no characteristic peaks in the mass spectrum, opposite to gold coating, we introduced a double-sided carbon coating in the substrate preparation protocol.

The thin sample preparation fails in several specific cases, when sample cannot be prepared in the form of very thin slices, e.g., human hair [34]. Therefore, the co-existence of both, continuous and pulsed, primary beam modes will still be necessary in order to suit most of the possible research interests.

Lateral and Mass Resolution

After the CEM detector was installed inside the microprobe vacuum chamber, its operation was tested with 5.8 MeV $^{35}\text{Cl}^{6+}$ primary ion beam.

The fine settings of currents driving the magnetic quadrupole lenses at the microprobe were optimized by scanning the beam over the reference copper mesh with 2000 periods/in., which is equal to 12.7 $\mu\text{m}/\text{period}$. In the high-current beam mode required for the MeV-SIMS with the pulsed primary beam, focusing is done with heavy ion PIXE (HI-XE) method, where the emission of Cu $L\alpha$ X-rays is detected as a function of the beam position. At the primary ion beam fluxes of 5000 ions/s, the yield of the induced X-rays is four orders of magnitude lower and could not be used. The beam size is in this case optimized by the CEM detector positioned behind the sample. The mesh bars stop completely the primary beam, whereas in the aperture region, the ion beam is transmitted and detected by CEM. A negative image of the mesh appears and can be well used to focus the beam (Figure 2).

With the object and collimating slits aperture values, which provide the primary ion fluxes of 5000 ions/s suitable for the MeV-SIMS continuous mode, we obtained sub-micrometer beam size. The optimal size of the brighter 5 MeV $^{35}\text{Cl}^{5+}$ beam is approx. $600 \times 800 \text{ nm}^2$ in horizontal and vertical dimensions, respectively. In the case of more frequently used 5.8 MeV $^{35}\text{Cl}^{6+}$ primary beam, the obtained optimal beam size is $800 \times 900 \text{ nm}^2$.

At the incoming primary ion frequency of 5 kHz, this in average is equal to 1 ion arrival at the sample per 200 μs . The duration of our time-of-flight measurement cycle is 100 μs . Under this conditions, obeying the Poisson statistics, there is approx. 30% probability of additional arrival of a random single ion within the TOF cycle, and approx. 8% probability for the arrival of two additional primary ions. The acquisition system ignores the arrival of these “random” ions, as the “start”

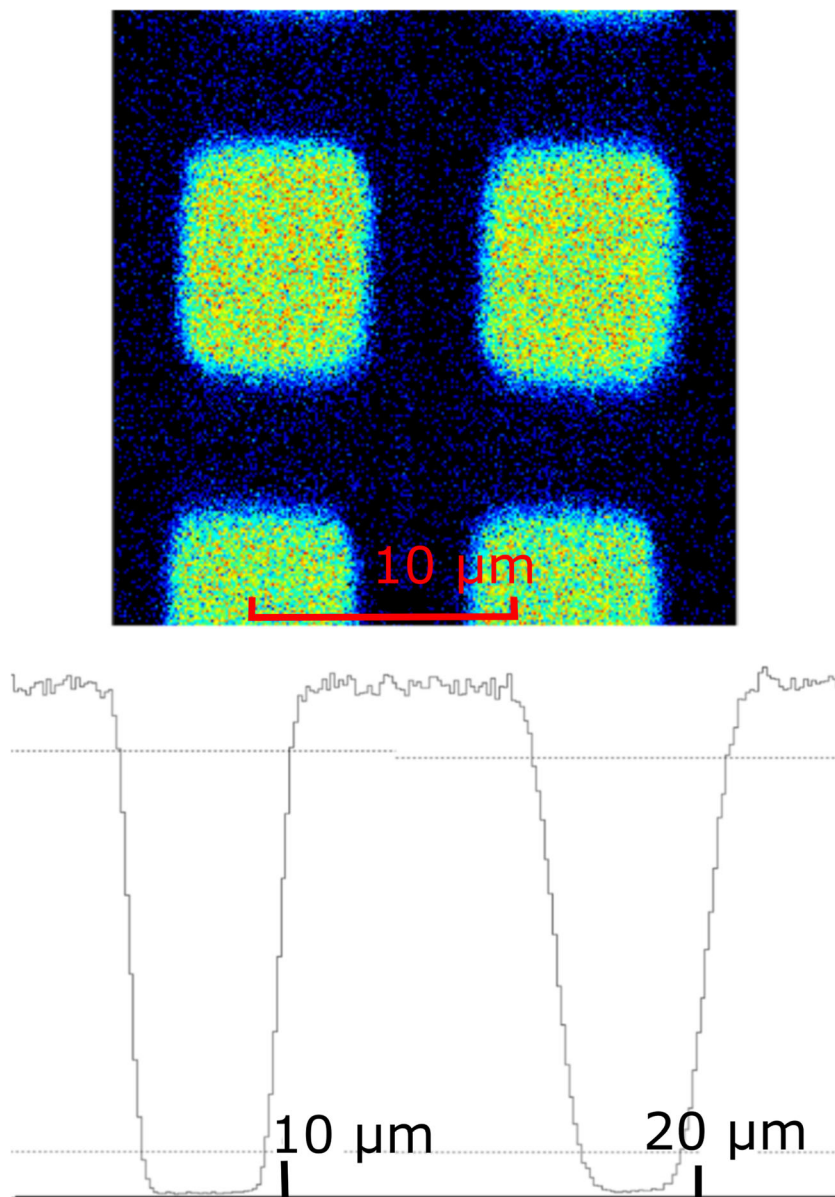


Figure 2. The negative image of 2000 periods/in. copper mesh and the beam profile along the x (left) and y (right) axes of the mesh, using the Cl^{6+} beam. The high count range represents the holes of the mesh, while the low count area represents the copper borders. The beam resolution is estimated via the knife edge method to approx. 800×900 nm, which is similar to PIXE abilities

detection is inhibited during the duration of the TOF cycle. Due to a random, time uncorrelated formation of secondary ions by these random primary ions, additional “stop” signals are triggered and associated with a random mass of secondary ion. This results in the formation of uniform background in the time (mass) spectra (Figure 3).

To deter the occurrence of the random background in the mass spectra, we applied the existing deflection plate system to blank the beam after the detection of each individual primary ion for a period of the duration of the TOF cycle ($100 \mu\text{s}$). Figure 3 demonstrates in logarithmic scale the occurrence of substantial uniform background in the mass spectra of leucine, when the frequency of the primary ions in the continuous primary beam is increased from 2 to 10 kHz. In addition, the

Figure 3 shows the effect of the primary beam stopping on the background amplitude in the measured mass spectra.

According to the laws of the Poisson statistics, in the case of high count rate of 10 kHz, there are only 5000 primary ions triggering the TOF measurement. Remaining 5000 primary ions are bombarding the sample randomly; thus, the background contributes to 50% of count rate in this case. For lower current at 2000 primary ions per second, there are on average 1667 triggers of TOF per second; thus, the background contribution is lowered to 16.7%, and for even lower current of 500 ions per second, the background is lowered further to 4.8%. In the case when the primary ion beam of 10 kHz is blanked and the undesired primary ions have only $1.5 \mu\text{s}$ to enter the chamber (the time for 6 MeV Cl ions to get from the deflector

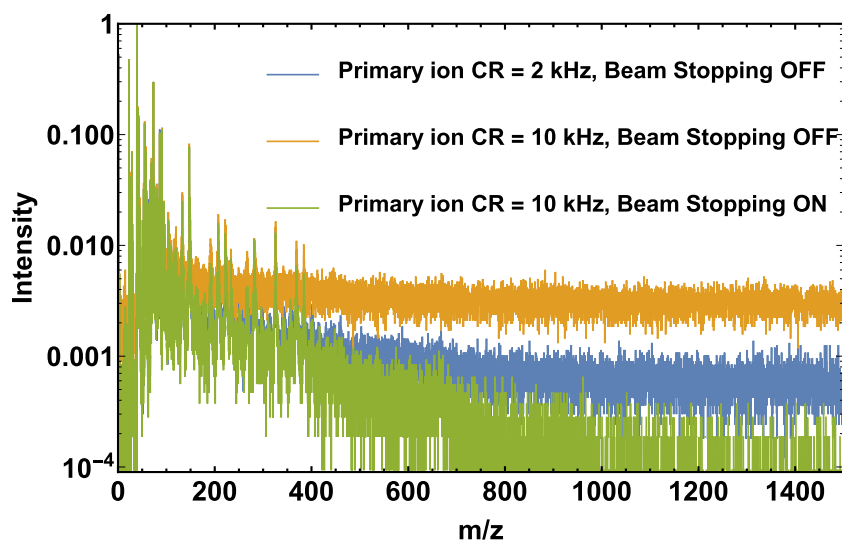


Figure 3. Comparison of spectra when beam blanke is turned on/off. In order to better demonstrate the effect of beam stopping, slits were open more than they usually are for low-current mode. Vertical scale is logarithmic

into the experimental chamber), until the beam deflector is turned on, the expected background contribution is reduced to 0.67%.

Experimental data are summarized in Table 1. We compared count rates in the last 60 and 12 μs of the time spectra, where most of the acquired events occur due to the background processes. An estimation of background contribution was then uniformly fitted over the rest of the TOF interval and compared with the results, predicted by Poisson statistics, which predicts the number of background events reasonably. Higher background values were measured experimentally.

Rough statistical analysis of the background contribution, as well as the appearance of the measured spectra with very weak background in comparison with the spectra acquired with a pulsed primary beam, indicates that we manage to detect the arrivals of the primary ions with an efficiency very close to 100%.

Afterwards, we acquired the reference spectra of amino acids and compared them with the spectra measured with pulsed primary beam (Figure 4). As expected, the mass resolution of spectra obtained by continuous primary ion beam improved substantially in comparison with the pulsed beam mode, as well as the peak-to-background ratio. The reason for better peak-to-background ratio in the continuous mode of operation is related with specifics of our beam pulsing approach, where we were not able to completely stop the arrival of random primary ions during the “beam off” conditions.

In the spectra acquired with continuous primary beam, the time width of several peaks in the time spectra is of the order of 4 ns, which is equal to the digitizing time of our analog-to-digital (ADC) conversion unit at the FPGA module used for data acquisition. The resulting mass resolution for the arginine peak ($m/z = 174.2$) is $m/dm = 800$ (in pulsed mode 300), and the hydrogen peak is accumulated within one channel in the time histogram, which brings us to the mass resolution limit of $m/dm = 300$ at the m/z value equal to 1. However, these values are dominantly determined by the digitizing time of ADC conversion unit. The mass resolution limit defined by physics is expected to be significantly higher and achievable by alternative acquisition hardware with shorter digitizing time.

As we are interested in further improvement of the mass resolution, we would like to estimate the physical constraints that would decisively limit the possible improvements. The initial energy dispersion of the desorbed molecular ions is expected to be the main physical constraint for further improvements of the mass resolution.

To compensate for the initial energy spread of the desorbed secondary ions, the delayed extraction mechanism was experimentally studied to further improve the mass resolution. The main idea behind delayed extraction protocol is to allow the desorbed ions freely drift in space for a definite time, without applying bias to the sample. After a definite time, bias is applied to the sample, and correspondingly, the kinetic energy to the secondary ions. Since the

Table 1. Number of counts in the last 12 and 60 μs of time spectra for the given primary ion current conditions. Background contribution was then estimated by fitting the background counts over the rest of the TOF interval and compared with the contribution predicted by Poisson statistics

	Total counts	Last 12 μs	Last 60 μs	Estimated background contribution (%)	Predicted background contribution (%)
CR = 500 Hz	103,327	1480	7938	11.9	4.8
CR = 2 kHz	648,178	23,113	120,215	29.7	17
CR = 10 kHz	705,700	58,003	290,690	68.5	50
CR = 10 kHz, blanked	366,824	368	6260	0.84	1.5

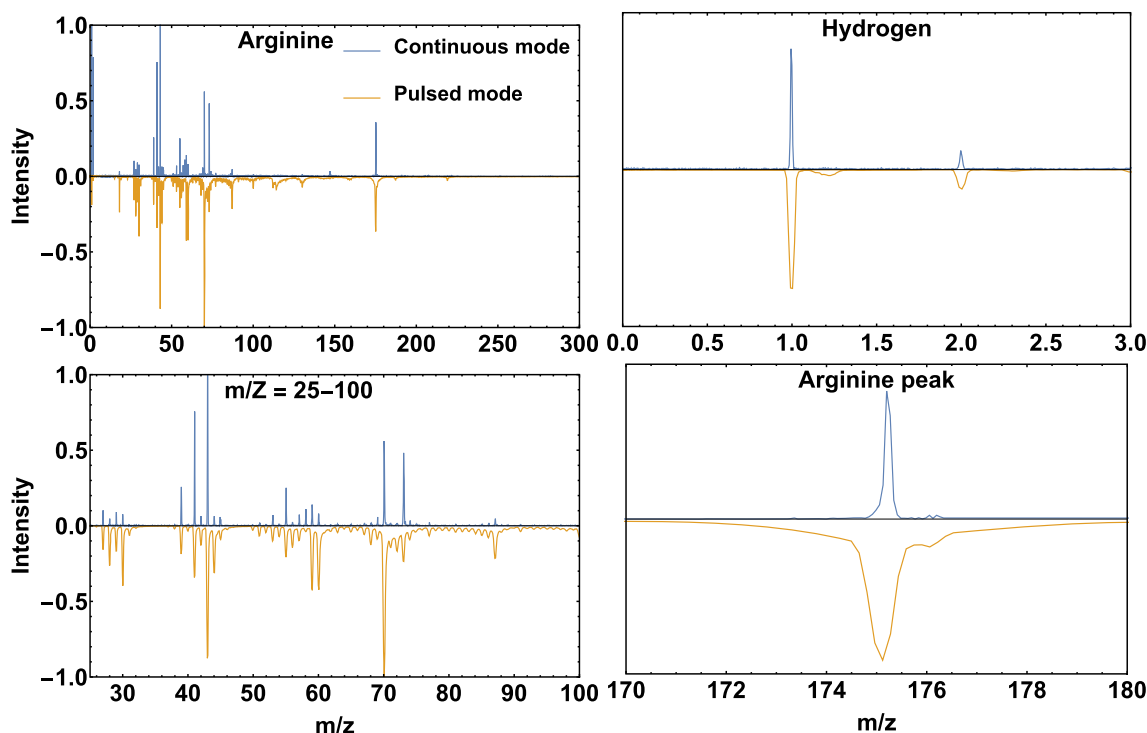


Figure 4. Comparison of amino acid (arginine) spectra obtained by bombarding the sample with continuous and pulsed $^{35}\text{Cl}^{6+}$ ion beam. The difference in peak-to-background ratio and in mass resolution can be clearly seen in all significant peaks. All spectra are normalized to potassium peak

ions with higher initial velocity will travel larger distance from the sample, they will receive less energy in the extraction gap between the sample and the spectrometer nozzle. Their TOF will in this way better match the TOF of initially slower molecules.

Experimentally, the implementation of time-delayed extraction mechanism proved to be very demanding using the existing instrumentation. The required rapid rise of the extraction voltage after the detection of the primary ion causes oscillations in the extraction voltage, as well as strong noise in the acquisition system, including series of false signals in the CEM. In order to diminish the noise in the system induced by the extraction pulses, the nozzle of the spectrometer was positioned further from the sample plane, resulting in a low secondary ion detection efficiency.

In our case, only a narrow and unstable combination of experimental parameters enabled the acquisition of high mass resolution spectra, presented in Figure 5. The optimal delay observed experimentally differs strongly from the calculated predictions based on the parameters of our spectrometer, where for the mass of 175 Da, estimation predicts optimum resolution at the delay below 100 ns. We observed a peaking of the mass resolution of the arginine molecular peak at the time delay value of 500 ns (Figure 5), where the mass width of a peak reached approx. half of the width without delayed extraction. Mass resolution at optimal time delay value for the molecular peak of arginine with the mass of 175 Da was estimated to reach a value of 1800 ± 150 .

The delayed extraction proved to have a promising potential in improving the mass resolution in the MeV-SIMS with TOF spectrometers; however, it turned out to represent a complex experimental endeavor, not completely solved within this work. Additional efforts need to be invested to solve experimental problems with the oscillation of the extraction voltage during its rise time and the mitigation of the strong associated noise in the channeltron detector, as well as in the entire acquisition system.

Biological Tissue Imaging

The motivation behind the present work was to improve both lateral and mass resolutions of MeV-SIMS for molecular mapping of the biological tissue at the cellular level. To demonstrate the characteristics of MeV-SIMS with continuous primary beam, we executed measurements on thin slices of biological tissue. The samples were prepared by colleagues at the Biotechnical Faculty of University of Ljubljana.

The preset cutting thickness at the cryotome was varied from 5 to 20 μm . After freeze-drying, the remaining thickness of selected samples fell to the values, where 5 MeV ^{35}Cl primary ions penetrated the tissue tilted for 55 angular degrees, providing the conditions for their chemical mapping with continuous primary beam MeV-SIMS.

Abundant presence of substances that provide structural integrity of the tissue after freeze-drying enabled thin slicing of the human liver tissue with uniform thickness. Frozen tissue

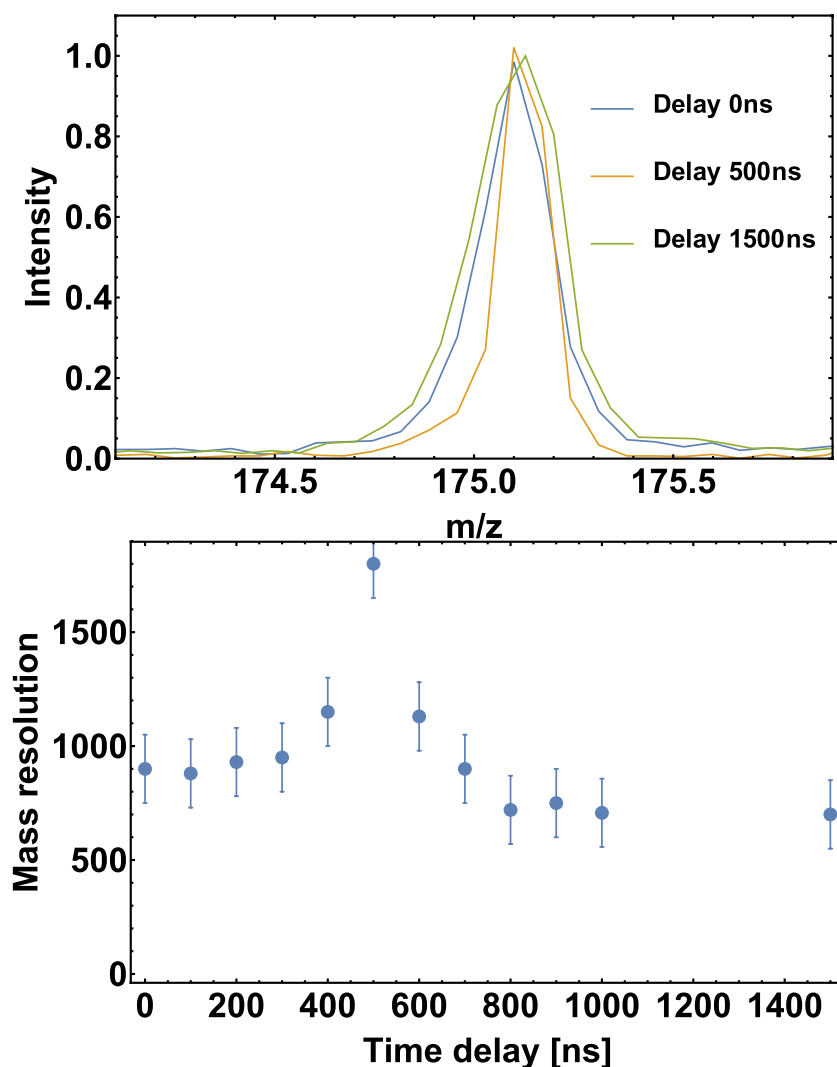


Figure 5. Shape of arginine molecule peak for three values of time delay (above), and measured values of mass resolution as a function of time delay

was sliced 5 μm thick on cryotome, freeze-dried, and deposited on the substrate consisting of 100 nm thick pioloform foil coated with 7 nm of carbon on both sides. The resulting dry tissue thickness was well below 2 μm , well suited for MeV-SIMS with continuous primary beam.

The comparison of human liver spectra demonstrates that the presence of the tissue does not impact mass resolution of the spectra, which remains approx. 800 for $m/z = 73$, compared to the mass resolution of 200 obtained with pulsed primary beam (Figure 6).

The difference in image quality between pulsed and continuous primary ion mode is also presented in Figure 6. While the resolution of 15 μm primary ion beam is barely enough to ensure the focused sample image sized 1.4×2.5 mm (x-axis is stretched due to the polar rotation of the sample), the image in continuous mode shows the potential for further zooming into the subcellular dimensions. Due to the homogeneity of molecular distribution in animal tissues, additional zoom on the human liver did not provide any additional valuable insights.

As evident in Figure 6, the count rate of secondary ions reflects the sample topography, as the local surface inclination influences the shape of the extraction field and, correspondingly, the number of detected primary ions from this location.

In our mapping, we would like to minimize the influence of the sample topography on the molecular yield. This could be achieved by several modes of yield normalization. The yield of selected molecular ion in each image pixel could be normalized to the total secondary ion yield in this particular pixel.

Alternatively, hydrogen yield is affected by the morphology, and as such also appropriate to normalize the molecular yields. Figure 7 demonstrates the proportionality between total ion and hydrogen signal at the corn seed tissue, presented in details later.

Normalizations on either hydrogen or total ion count have their significant pros and cons. In the case, when total ion count relies mostly on a few molecules, with their own preferential distribution, yield normalization of those molecules might overshadow the actual distribution. In this specific case, we can see that most of the molecules reside in the proximity to the

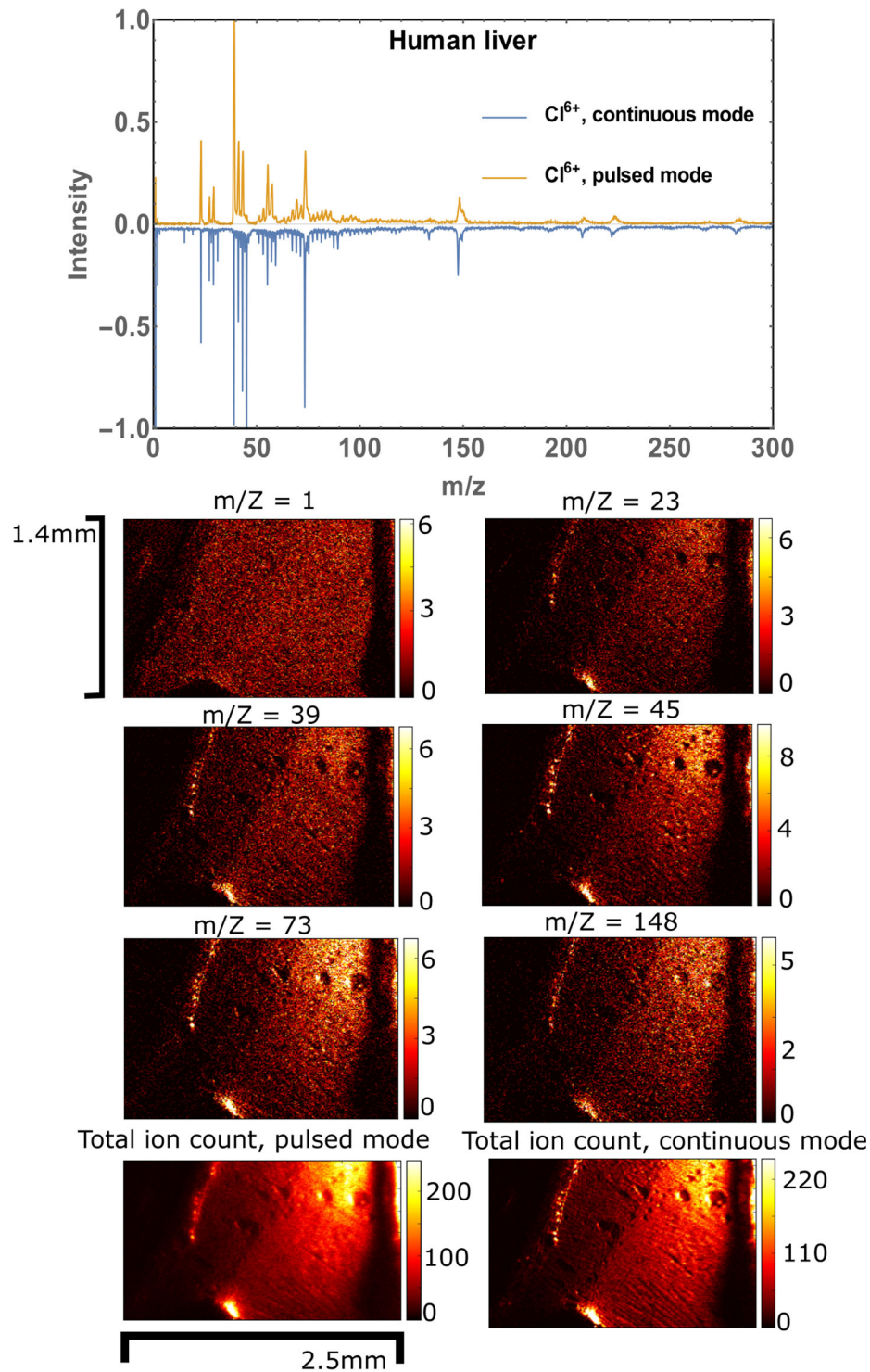


Figure 6. Total ion count and distributions of several peaks in the spectra of the human liver tissue. The comparison of images obtained by pulsed and continuous modes in the bottom line. In both cases, as well as in the cases of Figures 7 and 8, the sample was irradiated for 6 h at a steady current of approx. 3000–5000 primary ions/s. The corresponding fluence did not exceed 10^{10} ions/cm², which does not cause any significant damage to the samples according to our measurements [35]

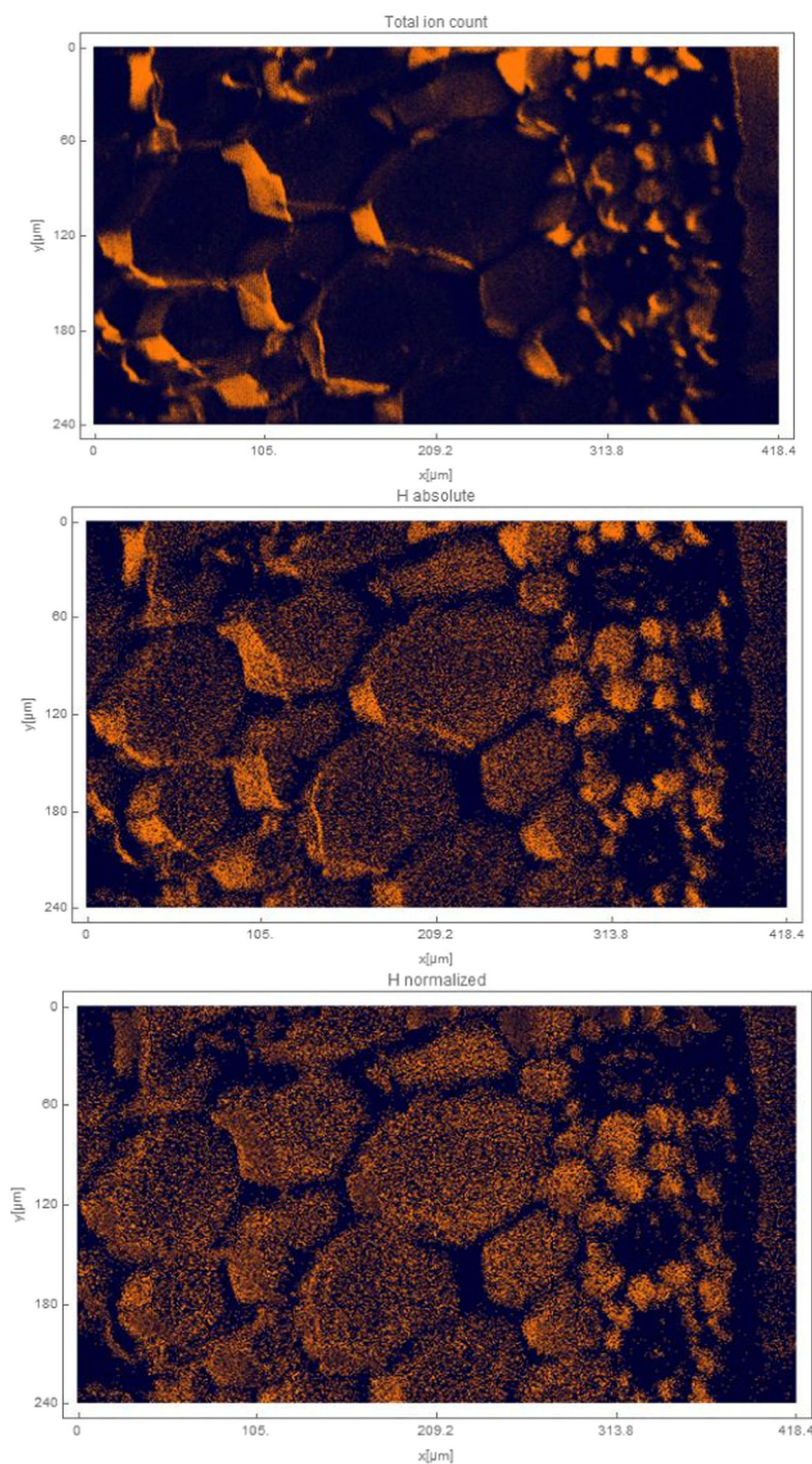


Figure 7. The topological effects have a significant effect on the signal strength, as can be seen on the total ion count image of the corn seed tissue. The strength of the hydrogen signal was found to be homogeneous besides the influence of topology. The bottom figure shows the ratio between total ion and hydrogen signal strengths. The resulting distribution is relieved from the inhomogeneity caused by the sample topography

cellular wall. On the other hand, hydrogen is often detected homogeneously throughout the biological sample, as is also the case here, and its signal strength solely depends on topological effects. However, the statistics of the hydrogen signal is

naturally worse than that of the total ion yield, which makes yield harder to normalize. If hydrogen signal is sufficient, we will normalize the yield of a particular molecular peak to the hydrogen signal.

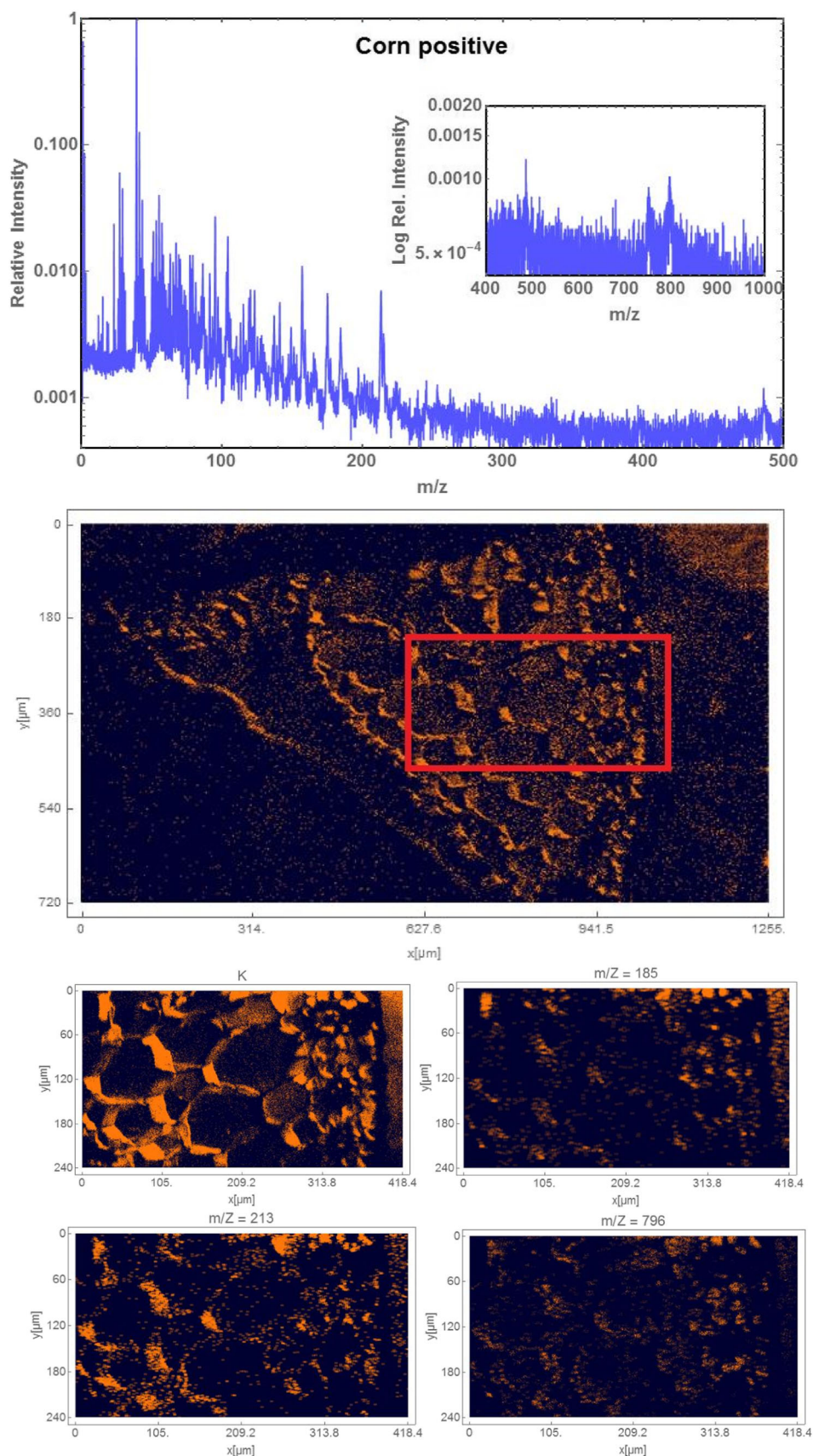


Figure 8. Spectra of the corn seed in logarithmic scale, normalized to the potassium peak ($m/z = 39$). Full-scanned total ion image is shown, as well as the distribution of several non-common molecular peaks in the zoomed area

Another set of measurements on biological samples was performed on corn seed tissue, prepared in the same manner as the human liver tissue. Thickness of corn seed samples was approx. 10 μm before drying in vacuum. We found that somewhat greater thickness of plant tissue is necessary due to the presence of cellular walls, which made the cutting process more challenging. Lesser thickness resulted in “empty” cells, whereas thickness above 7 μm provided similar molecular yield than the one obtained by measuring thick samples.

The most prominent peak in the spectra of corn seed (Figure 8) is potassium with $m/z=39$, which is common in plant tissues. Other significant, non-common peaks are at m/z ratios of 95, 157, 175, 185, 213, 215, 485, 750, and 796. Since the corn grain samples were exposed to several herbicides containing glyphosate ($m/z=169$) and glyphosate isopropylammonium salt ($m/z=228$), similar molecules were sought in the spectra and imaged across the sample (Figure 8).

The 2D distributions of those specific peaks vary from case to case. Some ions, including K and $m/z=213$, show equal distribution in both epidermal and mesophilic area, while their micro-location tends to be in the proximity of cellular walls. On the other hand, peaks such as $m/z=185$ and 796 clearly show preferential location in the epidermal region.

Conclusion

The development of MSI techniques is strongly motivated by the demands from the research in biology and medicine. The qualities of MeV-SIMS are well suited for the analysis of biological materials, as they offer the detection of biomolecules from chemically intact surface of the tissue. Since the elemental imaging by micro-PIXE has been intensively used by the biomedical community at JSI tandem accelerator, its lateral resolution of up to 600 nm served as a major targeting characteristic in the development of the MeV-SIMS to potentially complement the available elemental images with corresponding molecular images.

In our work, we reconfigured the mass spectroscopy approach by detection of the arrival of individual primary ions. This resulted in better definition of the “start” signal for time-of-flight (TOF) spectrometry, as well as in the efficient use of time in the TOF spectrometry, allowing the use of low primary ion current. The reduction of the primary ion beam intensity by three orders of magnitude resulted in the reduction of primary beam size down to sub-micrometer dimension. The beam size in low-current mode depends on the type of the primary ion beam; however, both 5 MeV $^{35}\text{Cl}^{5+}$ and 5.8 MeV $^{35}\text{Cl}^{6+}$ beams can be focused to dimensions of less than 1 μm . Such proficient lateral resolution of MeV-SIMS competes with the most advanced MSI techniques. In this way, it represents significant breakthrough in comparison with earlier performance of MeV-SIMS with pulsed beam featuring the lateral resolution of 10–15 μm .

Regarding the lateral resolution, the MeV-SIMS method with continuous primary beam belongs to the world-class MSI techniques. This is not the case with its present mass resolution. While the improvement of the mass resolution in comparison with the previously used pulsed mode is significant, the realized mass resolution of about $m/dm=1000$ for masses of 500 Da is still inferior compared with the capabilities of many other MSI methods. By our estimates, there is approx. 5 ns of time uncertainty during TOF measurement caused by various instrumental and physical processes.

In addition, several characteristics of electronic sputtering process are limiting the quality of mass spectra, the most important being the initial velocity spread of secondary ions. The time-delayed extraction is a possible solution to mitigate the consequence of this spread on the mass resolution. Our efforts in implementing the time-delayed extraction have not provided consistent solution yet. The main reason for this difficulties arises from strong instrumental noise induced during the risetime of the extraction voltage.

The tissue sample preparation protocol for continuous MeV-SIMS mode was developed in collaboration with Biotechnical Faculty, University of Ljubljana. While preparation of thin reference samples is a rather straightforward task, the preparation of thin tissue slices for continuous primary beam MeV-SIMS represents more demanding challenge. At the end of the iterations, we succeed with the substrate consisting of 100 nm thick pioloform foil, with both surfaces coated by approx. 7 nm of carbon. Solutions of reference samples are afterwards spin-coated onto the substrate, while biological tissues are thinly cut with a cryotome, freeze-dried, and later deposited on the substrate. First tests of molecular imaging performed on the human liver tissue and corn seed tissue are promising and motivate the group to further delve into the existing molecular imaging ability at the cellular level.

Acknowledgements

The work at the Jožef Stefan Institute was supported by the Slovenian research agency (ARRS) grants J7-9398, N1-0090, P1-0112, I0-0005, P1-0212, and EU H2020 project no. 824096 “RADIATE.”

References

1. Caprioli, R.: Molecular imaging of tissue sections by mass spectrometry: looking beyond the microscope. *J. Biomol. Tech.* **23**, 58 (2012)
2. Ferguson, C.N., Fowler, J.M., Waxer, J.F., Gatti, R.A., Loo, J.A.: Mass spectrometry - based tissue imaging of small molecules. *Adv. Exp. Med. Biol.* **806**, 283–299 (2014)
3. Soltwisch, J., Kettling, H., Vens-Capell, S., Wiegmann, M., Muthing, J., Dreisewerd, K.: Mass spectrometry imaging with laser - induced postionization. *Science*. **348**, 211–215 (2015)
4. Bodzon-Kulakowska, A., Suder, P.: Imaging mass spectrometry: instrumentation, applications and combination with other visualization techniques. *Mass. Spectrom. Rev.* **35**, 147–169 (2016)
5. Prideaux, B., Stoeckli, M.: Mass spectrometry imaging for drug distribution studies. *J. Proteome.* **75**, 4999–5013 (2012)

6. Zhao, Y.S., Li, C.: Mass spectrometry imaging: applications in drug distribution studies. *Curr. Drug Metab.* **16**, 807–815 (2015)
7. Giordano, S., Zucchetti, M., Decio, A., Cesca, M., Fuso Nerini, I., Maiezza, M., Ferrari, M., Licandro, S.A., Frapolli, R., Giavazzi, R., Maurizio, D., Davoli, E., Morosi, L.: Heterogeneity of paclitaxel distribution in different tumor models assessed by MALDI mass spectrometry imaging. *Sci. Rep.* **6**, 39284 (2016)
8. Patel, E.: MALDI - MS imaging for the study of tissue pharmacodynamics and toxicodynamics. *Bioanalysis.* **7**, 91–101 (2015)
9. Bjamholt, N., Li, B., D'Alvise, J., Janfelt, C.: Mass spectrometry imaging of plant metabolites - principles and possibilities. *Nat. Prod. Rep.* **31**, 818–837 (2014)
10. Dong, Y., Li, B., Malitsky, S., Rogachev, I., Aharoni, A., Kaftan, F., Svatoš, A., Franceschi, P.: Sample preparation for mass spectrometry imaging of plant tissues: a review. *Front. Plant Sci.* **7**, 60 (2016)
11. DeBord, J.D., Smith, D.F., Anderton, C.R., Heeren, R.A., Paša-Tolić, L., Gomer, R.H., Fernandez-Lima, F.A.: Secondary ion mass spectrometry imaging of dictyostelium dilcoideum aggregation streams. *PLoS One.* **9**, e99319 (2014)
12. Barbacci, D. C., Roux, A., Muller, L., Jackson, S. N., Post, J., Baldwin, K., Hoffer, B., Balaban, C. D., Schultz, J. A., Gouty, S., Cox, B. M. and Woods, A. S.: Mass spectrometric imaging of ceramide biomarkers tracks therapeutic response in traumatic brain injury. *Chem. Neurosci.* **8**, 2266–2274 (2017)
13. Angelo, M., Sean, C., Bendall, S.C., Finck, R., Hale, M.B., Hitzman, C., Borowsky, A.D., Levenson, R.M., Lowe, J.B., Liu, S.D., Zhao, S., Natkunam, Y., Nolan, G.P.: Multiplexed ion beam imaging of human breast tumors. *Nat. Med.* **20**, 436–442 (2014)
14. Wickerman, J.C., Gilmore, I.: *Surface Analysis: the Principal Techniques*, 2nd edn., p. 688. Wiley, Hoboken (2009)
15. Takats, Z., Wiseman, J.M., Gologan, B., Cooks, G.: *Science.* **306**, 471–473 (2004)
16. Wickerman, J.C.: *Analyst.* **136**, 2199 (2011)
17. Vestal, M.L.: *Hizrbak if Nass Socetrinetry*, vol. 44, pp. 303–317 (2009)
18. Laiko, V.V., Taranenko, N.I., Berkout, V.D., Yakshin, M.A., Prasad, C.R., Lee, H.S., Doroshenko, V.M.: *J. Am. Soc. Mass Spectrom.* **13**, 354–361 (2002)
19. Fletcher, J.S., Conian, X.A., Jones, E.A., Biddulph, G., Lockyer, N.P., Vickerman, J.C.: TOF-SIMS analysis using C60. Effect of impact energy on yield and damage. *Anal. Chem.* **78**, 1827–1831 (2006)
20. Rabbani, S., Barber, A.M., Fletcher, J.S., Lockyer, N.P., Vickerman, J.C.: TOF-SIMS with argon gas cluster ion beams: a comparison with C60+. *Anal. Chem.* **83**, 3793–3800 (2011)
21. Alford, T.L., Feldman, L.C., Mayer, J.W.: *Fundamentals of Nanoscale Film Analysis*. Springer, Berlin (2007)
22. Nakata, Y., Ninomiya, S., Matsuo, J.: Secondary ion emission from biomolecular thin films under ion bombardment. *Nucl. Inst. Methods Phys. Res. B.* **256**, 489–492 (2007)
23. Nakata, Y., Honda, Y., Ninomiya, S., Seki, T., Aoki, T., Matsuo, J.: Matrix-free high-resolution imaging mass spectrometry with high-energy ion projectiles. *J. Mass Spectrom.* **44**, 128–136 (2009)
24. Hedin, A., Hakansson, P., Sundqvist, B.: *Phys. Rev. B.* **31**, 1780–1787 (1985)
25. Sigmund, P.: *Fundamental Processes in Sputtering of Atoms and Molecules*, p. 675. Copenhagen, Kongelige Danske videnskabernes selskab (1993)
26. Jones, B.N., Matsuo, J., Nakata, Y., Yamada, H., Watts, J., Hinder, S., Palitsin, V., Webb, R.: Comparison of MeV monomer ion and keV cluster ToF-SIMS. *Surf. Interface Anal.* **43**, 249–252 (2011)
27. Nakata, Y., Honda, Y., Ninomiya, S., Seki, T., Aoki, T., Matsuo, J.: Yield enhancement of molecular ions with MeV ion-induced electronic excitation. *Appl. Surf. Sci.* **255**, 1591–1594 (2008)
28. Jeromel, L., Siketić, Z., Ogrinc - Potočnik, N., Vavpetič, P., Rupnik, Z., Bučar, K., Pelicon, P.: Development of mass spectrometry by high energy focused heavy ion: MeV - SIMS with 8 MeV Cl¹⁷⁺ beam. *Nucl. Inst. Methods Phys. Res. B.* **332**, 22–27 (2014)
29. Pelicon, P., Podaru, N.C., Vavpetič, P., Jeromel, L., Ogrinc Potičnik, N., Ondračka, S., Gott dang, A., Mous, D.M.: A high brightness proton injector for the Tandetron accelerator at Jožef Stefan Institute. *Nucl. Inst. Methods Phys. Res. B.* **332**, 229–233 (2014)
30. Vavpetič, P., Vogel-Mikuš, K., Jeromel, L., Ogrinc-Potočnik, N., Pongrac, P., Drobne, D., Pipan Tkalec, Ž., Novak, S., Kos, M., Koren, Š., Regvar, M., Pelicon, P.: Elemental distribution and sample integrity comparison of freeze-dried and frozen-hydrated biological tissue samples with nuclear microprobe. *Nucl. Inst. Methods Phys. Res. B.* **348**, 147–151 (2015)
31. Detterbeck, A., Pongrac, P., Rensch, S., Reuscher, S., Pečovnik, M., Vavpetič, P., Pelicon, P., Holzheu, S., Kraemer, U., Clemens, S.: Spatially resolved analysis of variation in barley (*Hordeum vulgare*) grain micro-nutrient accumulation. *New Phytol.* **211**, 1241–1254 (2016)
32. Vavpetič, P., Pelicon, P., Vogel-Mikuš, K., Grlj, N., Pongrac, P., Jeromel, L., Ogrinc - Potočnik, N., Regvar, M.: Micro-PIXE on thin plant tissue samples in frozen hydrated state: a novel addition to JSI nuclear microprobe. *Nucl. Inst. Methods Phys. Res. B.* **306**, 140–143 (2013)
33. Siketić, Z., Bogdanović Radović, I., Jakšić, M., Popović Hadžija, M., Hadžija, M.: Submicron mass spectrometry imaging of single cells by combined use of mega electron volt time-of-flight secondary ion mass spectrometry and scanning transmission ion microscopy. *Appl. Phys. Lett.* **107**, 093702 (2015)
34. Cloete, K.J., Jenčič, B., Šmit, Ž., Kelemen, M., Mkentanee, K., Pelicon, P.: Detection of lithium in scalp hair by time - of - flight secondary ion mass spectrometry with high energy (MeV) primary ions. *Anal. Methods.* **9**, 5249–5253 (2017)
35. Jenčič, B., Jeromel, L., Ogrinc - Potočnik, N., Vogel - Mikuš, K., Kovačec, E., Regvar, M., Siketić, Z., Vavpetič, P., Rupnik, Z., Bučar, K., Kelemen, M., Kovač, J., Pelicon, P.: Molecular imaging of cannabis leaf tissue with MeV-SIMS method. *Nucl. Inst. Methods Phys. Res. B.* **371**, 205–210 (2016)